Mat. Res. Soc. Symp. Proc. Vol. 661 © 2001 Materials Research Society

# Polymer-Clay Nanocomposite Materials: Solution and Bulk Properties

GUDRUN SCHMIDT*, ALAN I. NAKATANI, PAUL D. BUTLER,
VINCENT FERREIRO, ALAMGIR KARIM, CHARLES C. HAN
Polymers Division and Center for Neutron Research
National Institute of Standards and Technology, Gaithersburg, Maryland 20899

## ABSTRACT

The influence of shear on viscoelastic polymer-clay solutions was investigated by means of small-angle neutron scattering (SANS) under shear. SANS measured the shear-induced orientation of polymer and platelets. With increasing shear rate an anisotropic scattering pattern developed. At higher shear rates, the scattering anisotropy increases due to the increased orientation of the clay platelets in the shear field. Cessation of shear leads to fast recovery demonstrating the system to be highly elastic. As a result of drying, these solutions produce translucent nanocomposite films with a microporous membrane character. Depending on the preparation and degree of polymer-clay film dispersion, it is possible to modify the morphology and elastic properties of nanocomposite materials. Atomic Force Microscopy (AFM) reveals the network character and the development of morphology as a function of polymer concentration. Preliminary SANS experiments on the films will be correlated to morphologies obtained from AFM.

## INTRODUCTION

The objective of this work is to investigate the influence of shear on the structure development of highly viscoelastic, aqueous polymer-clay solutions. Here, we use SANS to study the shear orientation. Many models have been proposed for such solutions [1, 2, 3], but little is definitively known about the mesoscopic properties or shear behavior[1, 3]. This information is important in the production of nanocomposite materials.

Nanocomposite polymeric materials offer unique mechanical, electrical and thermal properties. Such property enhancements are induced not only by the physical presence of the filler, but also by the interaction of the polymer with the filler and the state of dispersion [4, 5, 6, 7, 8]. Most reinforcing agents, such as fibers and fillers, are large and scatter light, thus reducing light transmittance. In our studies efficient particle dispersion combined with good interfacial adhesion is achieved in aqueous polymer clay solutions. This property is maintained in the bulk material, which is the main reason for transparency. From a practical viewpoint, this allows the exciting possibility of developing strong yet transparent films, coatings and membranes from the solution.

## MATERIALS

In the following, we study a solution of the synthetic hectorite type clay, Laponite LRD (Laporte Industries Ltd.) [9], and poly(ethylene-oxide) (PEO) ($M_w = 10^6$ g/mol) [9, 10]. The results reported are for a highly viscoelastic solution containing a mass fraction of 3 % LRD and 2 % PEO (LRD2) at ambient temperature. The clay particles produce

transparent dispersions of disk shaped particles ≈ 300 Å in diameter and ≈ 10 Å thick [11, 12]. The pH and ionic strength of the solutions were controlled by the addition of NaOH and NaCl, respectively.

Upon drying, polymer clay solutions produce transparent nanocomposite films with micro-porous membrane character and elastic properties. These films were cast from solutions containing 95% water. AFM and SANS experiments were performed on 2 polymer-clay nanocomposite samples, bulk-LRD2 (mass fractions: 40 % PEO, 60 % clay) and bulk-LRD5 (60 % PEO, 40 % clay).

## RESULTS AND DISCUSSION

SANS measurements were made on the 30 m SANS instrument on NG7 at the National Institute of Standards and Technology Center for Neutron Research [13]. The shear cell used for the solutions is a Couette geometry, which has been described previously [14]. The cell has an inner diameter of 60 mm and a gap of 0.5 mm giving a total path length of 1 mm through the sample. In the standard configuration, referred to as the "radial beam" geometry, the incident beam is parallel to the shear gradient. In a second configuration, referred to as the "tangential beam" geometry, the incident beam is parallel to the flow direction. A sample to detector distance of 11.25 m and an incident wavelength, $\lambda$, of 9 Å was used to give a q range ($q=4\pi/\lambda \sin(\theta)/2$) of 0.0027 $Å^{-1} < q <$ 0.0199 $Å^{-1}$. The primary contrast in the SANS experiment is between $D_2O$ and the other solution components (clay, PEO, salts), thus SANS experiments can detect the orientation of the clay platelets and polymer chains under shear. We will refer to these samples as "regular" ones. SANS on contrast matched samples (to clay) detect only the orientation of the polymer.

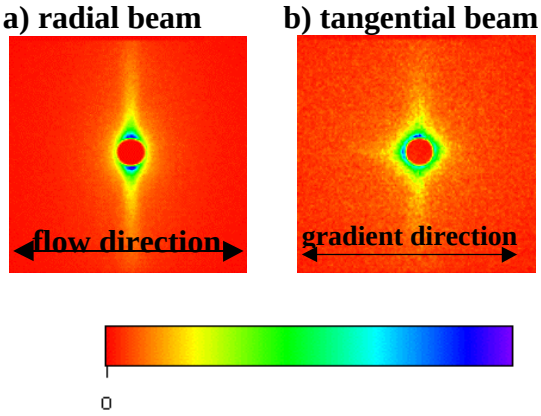


Figure 1. a) SANS patterns from LRD2 in the a) radial geometry and b) tangential geometry at a shear rate of 90 $s^{-1}$. Anisotropy in gradient direction (b) comes from reflections due to the empty Couette cell. The apparent anisotropy is lower in the tangential beam due to the distribution of platelets caused by the curvature of the shear cell in the tangential scattering geometry.

Results (raw data) as obtained from the polymer-clay solutions in the "radial" and "tangential" beam configurations are summarized in Figure 1. SANS data indicate the flow is strong enough and alignment increases continuously with shear rate. Platelets can be oriented in three different ways: 1). with the surface normal along the velocity

direction, 2). with the surface normal along the flow direction and 3). with the surface normal along the neutral direction. According to SANS patterns from both beam configurations (Figure 1) the shear flow results in an alignment of clay platelets. The platelets are oriented in the flow direction with the surface normal in the neutral direction [15]. This orientation is also occasionally observed in liquid crystalline lamellar phases [16], block copolymer solutions[17] and melts [18].

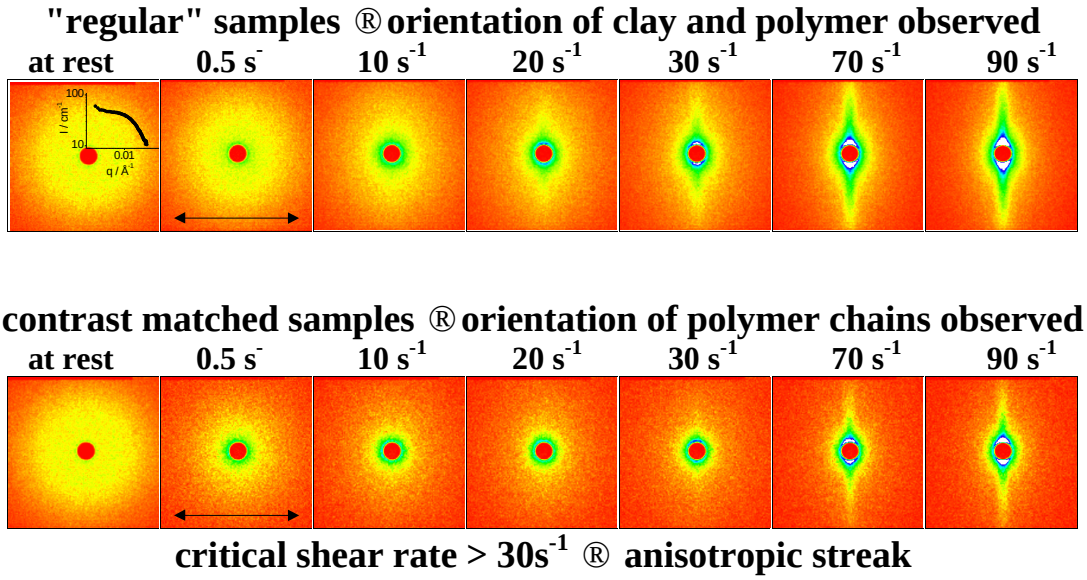


Figure 2. Radial beam configuration: Two dimensional SANS profiles obtained from LRD2 regular samples (first series) and LRD2 contrast matched samples (second series).

SANS results obtained from regular and contrast matched samples are shown in Figure 2. With the sample at rest (regular samples) a maximum in scattering intensity was observed which broadens at low shear rates (Fig. 2, regular sample). The maximum corresponds to an average spacing between platelets $q_{max} \approx 0.007$ Å$^{-1}$, ($d = 2\pi/q_{max}$ = (900 to 1100) Å). With increasing shear rate, the maximum disappears and we observe a systematic increase of anisotropic scattering intensity (streak) perpendicular to the flow direction. For contrast matched samples, significant SANS anisotropy in scattering develops only at 30 s$^{-1}$ and higher.

To account for the SANS results, our current understanding is that the polymer chains are in a dynamic adsorption/desorption equilibrium with the clay particles to form a network. The peak position in the quiescent scattering pattern is an indication of the mesh size of this network (≈ 1000 Å). A 2 % (mass fraction) solution of only PEO, at the same pH, polymer and salt concentration, showed no anisotropic SANS scattering at shear rates up to 100 s$^{-1}$. Similarly a 3 % (mass fraction) aqueous clay solution shows no evidence of an anisotropic SANS pattern. Therefore, we can conclude that the anisotropic SANS pattern observed in the clay-polymer solutions is due to this coupling between clay platelets and polymer, allowing a higher orientation than either single component in solution can produce. From SANS data on "regular samples" we determine the clay particles orient first at low shear rates. Significant orientation of the PEO (contrast-matched samples) occurs much later, above shear rates of ≈ 30 s$^{-1}$. Since the clay platelets

and the PEO chains are of comparable size (both about 300 Å), the lack of internal flexibility of the rigid clay particles makes them much easier to align than the flexible polymer chains.

On cessation of shear, the stress on the network decays almost immediately, and the recovery of the isotropic structure is controlled by the relaxation of the stretched chains. As the chains retract, the coupling of the chains to the clay allows the platelets to randomize in orientation under the local viscous environment.

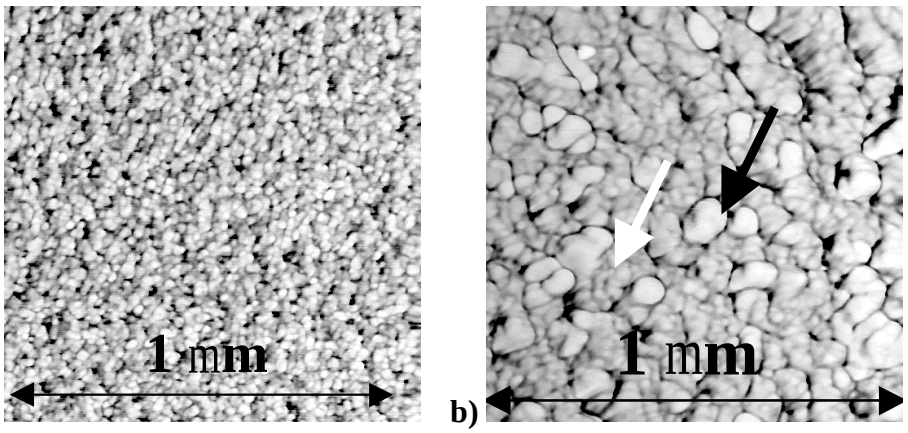


Figure 3. AFM phase images of a) bulk-LRD2 and b) bulk-LRD5 film morphology (1μm x 1μm). One dot in figure 3a corresponds to ca. 300 Å in diameter, which is the dimension of one clay platelet.

Upon drying, polymer clay solutions produce transparent nanocomposite films with a micro-porous membrane character and elastic properties. These films (thickness ≈ 5 μm) were cast from solutions containing 95% water. We expect that AFM of the dried film may even provide insight into the network character of the polymer in solution. Most reinforcing agents, such as fibers and fillers are large and scatter light, thus reducing light transmittance. Efficient particle dispersion combined with good interfacial adhesion is achieved in the aqueous polymer clay solution and this property is maintained in the film. This is the main reason for transparency. From a practical viewpoint, this allows the exciting possibility of developing strong yet transparent films, coatings and membranes from solution.

All AFM experiments were carried out using a Dimension 3100 microscope from Digital Instruments operating in Tapping Mode [9]. This mode allows us to distinguish between soft PEO and hard clay. AFM images of the pure LRD film (not shown here) show clay particles, which lie flat on the surface [19]. The average diameter of the clay platelets is about 300 Å, which is consistent with previous SANS[15] experiments and published literature [3]. By drying LRD2 we obtain a film with mainly clay particles which are randomly oriented and connected by polymer (Figure 3a). LRD5 dried film exhibit two areas with quite different representative structures (Figure 3b). The first structure is a mesoporous homogeneous film texture with same size particles. The second structure shows a heterogeneous structure (Figure3b): 1) areas where clay particles are agglomerated (white arrow) and 2) areas where only excess PEO (black arrow) is observed. In both cases the polymer acts as a connection between particles. LRD2 produces an elastic porous film with mainly clay particles, which are connected by

polymer and randomly oriented (Figure 3a). LRD2 dried films exhibit spherical particles, which each particle having the same average diameter compared to one clay platelet (Figure 3a).

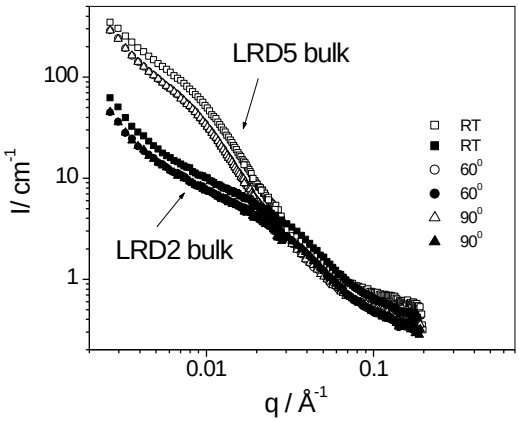


Figure 4. Temperature and concentration dependence of SANS intensity from 2 polymer-clay nanocomposite samples. Bulk-LRD2 (40 % PEO, 60 % clay) and bulk-LRD5 (60 % PEO, 40 % clay). Relative standard deviation: ca. 4 %.

In contrast to bulk-LRD2, some areas of bulk-LRD5 films show domains with excess of PEO. These domains are the white "dots" in Figure 3b (black arrow). LRD5 solutions studied by SANS and flow birefringence [15] show exfoliated clay particles and well dispersed PEO. AFM investigations of these bulk-LRD5 dried films show that this composition appears to be the critical concentration where a transition from a homogeneous network like structure to a heterogeneous structure occurs. The excess PEO does not contribute to building the network. A more detailed study around this critical concentration will be made in the future. With increasing PEO mass fraction beyond a value of 5 % in a solution, the number and the size of PEO "dots" in a dried film increases, and no isolated clay platelet can be observed since the clay platelets are all polymer covered. In all cases the polymer provides strong connections between clay particles as has been shown by rheology experiments [20]. Moreover, after annealing the films at 50 °C or after isothermal crystallization in order to crystallize the PEO, no morphological modifications were observed. Additional DSC experiments on bulk-LRD2 sample shows no crystallization peak in a range of (30 to 200°)C. These results indicate that there is not enough PEO chain mobility to crystallize because of the strong interactions with the clay fillers within the network. Upon annealing far above the melting temperature of PEO ($T_m$ = 71 °C) the bulk-LRD2 film shows no dewetting and is stable for hours suggesting there is no degradation of the polymer or film properties.

Preliminary SANS results on both bulk-LRD2 and bulk-LRD5 films are shown in Figure 4. For both concentrations we observe no significant temperature dependence up to 100 $^{o}$C. In the high q-range no significant concentration dependence is detected although AFM images show quite different textures. In the low q-range however strong concentration dependence is visible, which may be correlated with the morphology as observed in AFM (Figure 3).

## SUMMARY

The influence of shear on viscoelastic polymer-clay solutions was investigated by means of small-angle neutron scattering (SANS) under shear. Polymer chains are in dynamic adsorption/desorption equilibrium with the clay particles to form a network. Under shear we observe an unusual alignment of clay platelets along the flow direction with the surface normal in neutral direction. SANS on regular samples measured the shear-induced orientation of polymer and platelets. SANS on contrast matched samples detected the orientation of the polymer alone. With increasing shear rate clay particles seem to orient first (SANS on regular samples) then polymer chains start to stretch (SANS on contrast matched samples). Cessation of shear leads to fast recovery demonstrating the system to be highly elastic.

As a result of drying, polymer-clay solutions produce translucent nanocomposite films with a microporous membrane character. Preliminary AFM experiments exhibit different morphologies as a function of polymer concentration. AFM images the network character and the development of morphology as a function of polymer concentration. Future SANS experiments on several concentrations will be correlated to morphologies as obtained from AFM.

## ACKNOWLEDGMENTS

Financial support by the Alexander von Humboldt Foundation is greatfully acknowledged by Gudrun Schmidt.

## REFERENCES

1. A. Mourchild, A. Delville, J. Lambard, E. Lecolier, P. Levitz, *Langmuir* , 1942 (1995).
2. H. J. M. Hanley, G. C. Straty, F. Tsvetkov, *Langmuir* , 3362 (1994).
3. F. Pignon, A. Magnin, J. M. Piau, *J. Rheol.* **42**, 1349 (1998).
4. T. Lan, T. Pinnavaia, *J. Chem. Mater.* , 2216 (1994).
5. Z. Wang, T. Pinnavaia, *J. Chem. Mater.* , 1820 (1998).
6. A. Usuki, M. Kawasumi, Y. Kujima, A. Okada, *J. Mater. Res.* **8**, 1174 (1993).
7. Y. Kojima, et al., *J. Mater. Res.* **8**, 1179 (1993).
8. R. A. Vaia, *Structural Characterization of Polymer Layered Silicate Nanocomposites*. T. J. Pinnavaia, G. W. Beal, Ed., Polymer-Clay Nanocomposites (John Wiley and Sons, New York, 2000).
9. *Certain equipment and instruments or materials are identified in this paper in order to adequately specify the experimental details. Such identification does not imply recommendation by the National Institute of Standards and Technology nor does it imply the materials are the best available for the purpose. .*
10. *According to ISO 31-8, the term "Molecular Mass" has been replaced by "Relative Molecular Mass", symbol Mr. Thus, if this nomenclature and notation were to be followed, one would write, Mrw, instead of the historically conventional Mw for the mass average molecular weight and it would be called the "Mass Average Relative Molecular Mass". The conventional notation rather than the ISO notation has been employed for this publication.*
11. J. D. F. Ramsay, S. W. Swanton, J. Bunce, *J. Chem.. Soc., Faraday Trans.* , 3919 (1990).
12. F. Pignon, et al., *Phys. Rev. E* **56**, 3281 (1997).
13. C. J. Glinka, et al., *J. Appl. Cryst.* , 430 (1998).
14. G. C. Straty, H. J. M. Hanley, C. J. Glinka, *J. Statistical Physics* **5/6**, 1015 (1991).
15. G. Schmidt, A. I. Nakatani, P. D. Butler, A. Karim, C. C. Han, *Macromolecules* **33**, 7219 (2000).
16. D. N. Roux, F.; Diat, O., *Europhys. Lett.* **24**, 53 (1993).
17. S. Kitade, et al., *Macromolecules* , 8083 (1998).
18. U. Wiesner, *Macromol. Chem. Phys.* **198**, 3319 (1997).
19. V. Ferreiro, G. Schmidt, C. C. Han, A. Karim, *ACS Nanocomposite Symp. Proceedings* (2000).
20. G. Schmidt, A. I. Nakatani, C. C. Han, *Rheol. Acta* , submitted (2001).